GEOPHYSICS, VOL. 84, NO. 4 (JULY-AUGUST 2019); P. D171–D177, 12 FIGS., 1 TABLE.
10.1190/GEO2018-0464.1

Numerical study of the effect of cement defects on flexural-wave logging

Ruolong Song[1], Hefeng Dong[2], and Xueshan Bao[3]

ABSTRACT

Cement-bond evaluation is needed for new wells and plug and abandonment activities. The ultrasonic leaky Lamb-wave (also called the flexural-wave) technique, in combination with the pulse-echo technique, has been widely used for cement-quality evaluation. Using a 2D time-domain staggered-grid stress-velocity finite-difference methodology, we have numerically investigated the attenuation and group velocity of flexural waves, and the scattering from defects, in the presence of a water-filled void in the cement annulus. The position, length, thickness, and burial depth of a defect are considered. The numerical study suggests that the combination of the attenuation and group velocity of the flexural wave allows for a discrimination between solids and liquids. The scattering from voids can be used to indicate the existence of a hidden defect, which cannot be detected by using the attenuation and group velocity if it is located larger than 5 mm away from the casing. The void signatures can even be used to characterize the geometry of the defect for neat cement. The numerical results provide improved understanding of flexural-wave logging results.

INTRODUCTION

The combination of the ultrasonic flexural-wave method and the classical pulse-echo method is a promising approach for cement-bond evaluation (Zeroug, and Froelich, 2003; Kuijk et al., 2005; Froelich, 2008; Al-Suwaidi et al., 2009), especially for lightweight cement, which has been developed for cementing casings and liners in weak formations with a low fracture gradient to prevent fracturing and lost circulation while placing the cement slurry (Al-Suwaidi et al., 2001). The pulse-echo method can estimate the acoustic impedance (computed as the product of the density by compressional velocity) of the material immediately behind the casing with accuracy of 0.5 MRayls (Kuijk et al., 2005). Flexural-wave attenuation can be calculated from the amplitudes of wavefield first arrivals measured on two adjacent receivers. It first increases approximately linearly as the acoustic impedance behind the casing increases, and then it rapidly decreases when this impedance is greater than 4.7 MRayls (Froelich, 2008). The measured flexural-wave attenuation is more reliable than acoustic-impedance measurements in the intermediate range, where acoustic-impedance contrast between the fluid and lightweight cement is rather low. Based on the measured flexural-wave attenuation and acoustic impedance, the solid, liquid, and gas states of the material behind the casing can be estimated (Al-Suwaidi et al., 2009). This interpretation method assumes that the casing is intact and the material behind the casing is homogeneous. Zeroug (2004) presented an analytical forward model for simulating the interaction of ultrasonic flexural wave with a cylindrically layered fluid-loaded elastic structures. He et al. (2014) and Wang et al. (2016) numerically investigate the flexural-wave attenuation with the existence of a thin liquid-filled channel between the casing and the cement sheath. Tao et al. (2016) numerically study the response of flexural waves in the presence of defects within the casing and rough cement-formation interface. Xu and Hu (2017) calculate the shear velocity of cement using the reflected flexural wave, assuming a known cement thickness. If the material behind the casing is inhomogeneous, for example, there is a void filled with water in the cement. This situation could happen in practice. In this paper, we use a 2D finite-difference methodology to numerically study the effects of a water-filled void in cement annulus on attenuation, group velocity, and scattering of flexural waves.

In the following sections, we first introduce the finite-difference (FD) method and the 2D model. We then present the numerical simulations for different scenarios. Finally, we discuss the significance of the results in actual field test scenarios.

TWO-DIMENSIONAL MODEL

In cement-bond evaluation, the transmitter's operating frequency of flexural-wave logging is commonly 250 kHz. The wavelength of

Manuscript received by the Editor 7 July 2018; revised manuscript received 7 February 2019; published ahead of production 8 May 2019; published online 20 June 2019.
[1]Jilin University, College of Physics, Changchun, China. E-mail: songrl@jlu.edu.cn (corresponding author).
[2]Norwegian University of Science and Technology, Department of Electronic Systems, Trondheim, Norway. E-mail: hefeng.dong@ntnu.no.
[3]Great Wall Drilling Corporation, Logging Technology Institute, Beijing, China. E-mail: xueshan.bao@gmail.com.

P-waves in water, the fluid inside the casing, is approximately 0.6 cm. The diameters of the casing and borehole are normally 14 and 21 cm, respectively. The short wavelength allows the use of a planar-multilayered model to approximate the cylindrical-layered structure. The short wavelength also provides high circumferential resolution. When the channel width is no less than the diameter of the transducer, approximately 2.54 cm (1 in), a highly efficient 2D model can be used instead of a time-consuming 3D model. However, for a smaller channel, or for cases in which the transducers are facing the margin of a channel, a 3D model is needed.

In this study, we adopt the four-layer 2D model shown Figure 1 that mimics a steel-cased well filled with cement between the steel casing and the formation. The model size is 54×10 cm (excluding absorbing boundaries). The thicknesses of the layers from top to bottom are 3.2, 0.8, 4, and 2 cm, respectively. If there is a defect in cement layer, the defect will be filled with water. The transmitter is modeled by point force sources arranged in a line of 2 cm. To measure the leaky flexural wave, the transmitter and the two receivers have a tilt angle of 36° based on the phase velocity of flexural wave and Snell's law. The transmitter's center is located at (3, 1 cm). The transmitted signal is modeled as

$$g(t) = (1 + \cos(2\pi(t - t_c/2)/t_c)) * \cos(2\pi f_0(t - t_c/2)) * (H(t) - H(t - t_c)), \quad (1)$$

where $f_0 = 250$ kHz is the central frequency, $t_c = 3/f_0$ is the duration of the impulse, and $H(t)$ is the Heaviside step function. There are two receivers with a spacing of 10 cm, and the distance between the transmitter and the first receiver R1 is 30 cm. The two receivers are also line receivers that have the same length of the transmitter.

Table 1. Acoustic parameters of the 2D FD model.

Material	(kg/m^3)	(m/s)	(m/s)
Water	1000	1500	—
Steel casing	7800	5930	3250
Neat cement	1800	3200	1750
Lightweight cement	1250	2600	1300
Formation	2180	3960	2350

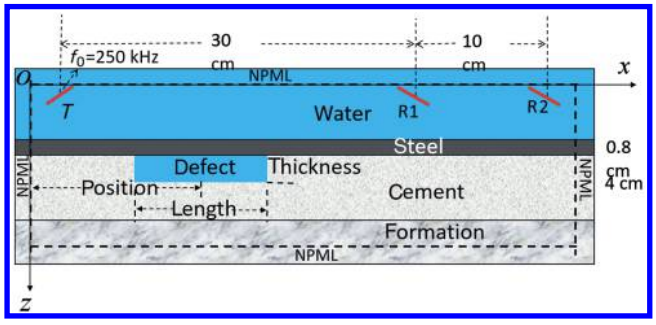

Figure 1. The 2D FD numerical model. T denotes the transmitter, and R1 and R2 denote receivers. A defect in the cement layer is defined by its length, thickness, and position (the x-coordinate of its center).

The recorded waveform is the mean value across the receiver line. Table 1 lists the acoustic parameters used in the simulations.

We use a fourth-order central-difference FD scheme in the spatial domain and a second-order central-difference formula in the temporal domain. The stress-velocity staggered-grid approach is used (Liu et al., 1996). The grid size is 0.5 mm, ensuring that at least 12 cells per minimum wavelength are used at the center frequency. The time step size is 0.05 μs. A smaller grid size and time step are used for special cases to ensure that there are at least four grid points in both directions for tiny defects. To eliminate artificial reflections from the boundaries of restricted computation region, the model is surrounded by nonsplitting perfectly matched layers (Wang and Tang, 2003) of 15-point width in the x- and z-directions. The simulation code is developed based on the previous works of the authors (Song et al., 2012).

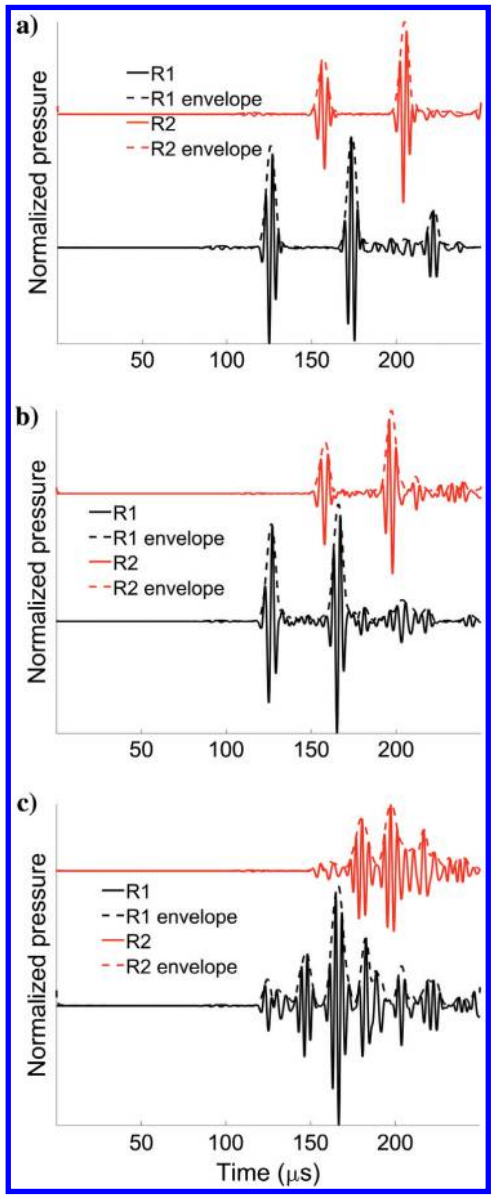

Figure 2. Simulated waveforms of the flexural-wave logging with homogeneous material behind casing. (a) Water, (b) neat cement, and (c) lightweight cement.

NUMERICAL RESULTS AND DISCUSSION

Homogeneous material behind the casing

We first simulate the cases with homogeneous material (no defect) behind the casing to study the influence of the material behind the casing on the received signals. The material in the first layer is water in all cases. The material behind the casing is water, neat class-G cement (neat cement for short) or lightweight cement. The slurry of neat cement is a mixture of water and cement. The slurry of lightweight cement is a mixture of water, cement, and silica microspheres (Al-Suwaidi et al., 2009). The acoustic parameters used in the simulations are listed in Table 1. The received waveforms by the two receivers are plotted in Figure 2. The first wave packet in the waveforms in Figure 2 is the primary flexural wave. For the case in which the cement layer behind the casing is filled with water shown in Figure 2a, the second wave packet is the reflected flexural wave from the cement-formation interface (the third interface). Because there is only P-wave in fluid, this reflection is the PP mode. It is also called the third interface echo (TIE) by Al-Suwaidi et al. (2009). For the case where the cement layer is filled with neat cement shown in Figure 2b, the second wave packet is SS mode, as the velocity of P-wave in neat cement is greater than the phase velocity of the flexural wave. The tangential (parallel to the interface) wavenumbers of each layer in multilayer structure must be identical based on Snell's law, so there is no P-wave propagating in the neat cement. For the case with a lightweight cement behind casing shown in Figure 2c, the waveforms are more complicated because the flexural wave radiates P- and S-waves into the cement (Kuijk et al., 2005). There are PP, PS/SP, and SS modes and their multireflected versions. The snapshots of the stress component τ_{xx} at 112 μs for the same models as in Figure 2 are shown in Figure 3. We see that the first wave package is zero-order symmetric mode (S0) in Figure 3a, which has the fastest velocity. The S0 mode leaks little energy outside the steel plate because the particle displacement is mainly along the x-direction. The following wave package is the zero-order antisymmetric mode (A0), also called the flexural wave. The A0 mode radiates into the fluid and the cement as a P-wave or/and an S-wave. These radiations into the cement can be reflected by the third interface and measured by the receivers inside the casing.

The flexural wave attenuates quickly as it propagating along the casing. The attenuation rate depends on frequency slightly in the operating frequency band. The attenuation in frequency domain shown in Figure 4 is obtained by comparing the Fourier transform of the first reflections between two receivers. We apply a 24 μs rectangular window before taking the Fourier transform. The results of the Fourier transform are sensitive to waveform distortion caused by

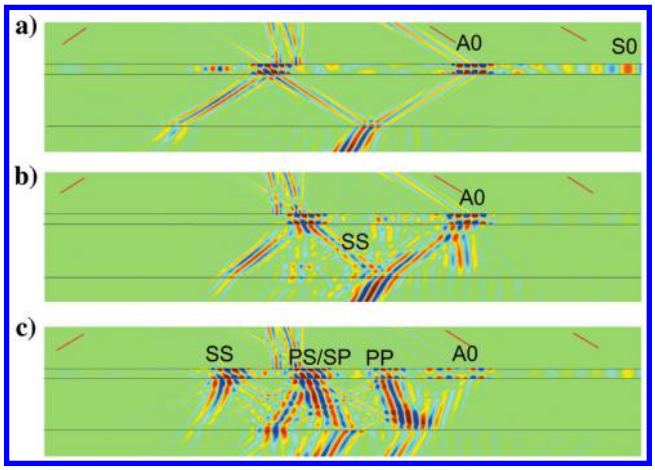

Figure 3. Snapshots of stress component τ_{xx} at 112 μs for the same models in Figure 2. The structure interfaces are overlaid with black lines, and the positions of the transmitter and receivers are indicated by red lines.

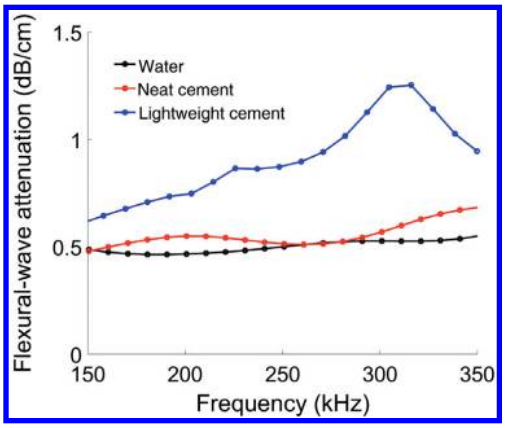

Figure 4. The flexural-wave attenuation in the frequency domain for the cases in Figure 2.

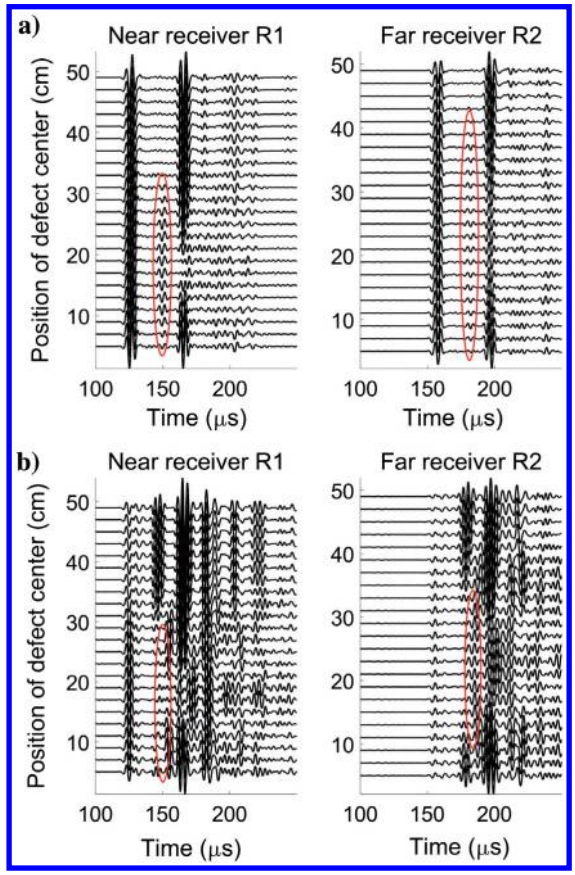

Figure 5. Simulated waveforms for a shifting defect packet in the cement next to the casing. (a) Neat cement and (b) lightweight cement.

reflected flexural waves and long tails of the S0 mode. The distortion may lead to an untrusted attenuation rate. Therefore, in this study, we calculate the flexural-wave attenuation in the time domain by comparing the amplitude of the first echo envelope between the two receivers using the approach of Al-Suwaidi et al. (2009). The envelope is obtained by taking the Hilbert transformation of the waveform. The calculated flexural-wave attenuations for water, neat cement, and lightweight cement behind casing are 0.51, 0. 62, and 1.02 dB/cm, respectively. These attenuations are due to the leakage of the flexural wave in the steel casing into both sides. The results are close to the theoretical flexural-wave attenuations at 200 kHz given by Kuijk et al. (2005). The group velocity of flexural wave can be calculated by using the time difference between the envelope peaks of first reflections. The group velocity of flexural wave is 3180, 3230, and 3280 m/s for neat cement, water, and lightweight cement behind the casing, respectively.

The effects of defect position

In this subsection, we investigate the flexural waves for the cases in which a water-filled void in the cement is placed next to the casing with changed positions (defined by the x-coordinate of the pocket center) along the casing-cement interface. The cement is neat cement or lightweight cement given in Table 1 and is well-bonded to the casing. The length and thickness of the defect are 10 and 2 cm, respectively. Figure 5 shows the simulated waveforms at the two receivers for different positions of the defect, Figure 5a for neat cement, and Figure 5b for lightweight cement. The waveforms are normalized by a fixed value. When the defect is located between the transmitter and receiver R1, the scatterings from the defect-cement and the cement-formation interfaces can be recorded by this receiver. In Figure 5a, for neat cement, the reflections in the red ellipse is the PP-mode reflected by the defect-cement interface; we call them defect scattering for short, and the following ones are the SS mode reflected by the cement-formation interface. In Figure 5b, for lightweight cement, the defect scatterings are still visible in between the PP and PS modes from the cement-formation interface. The defect scatterings bring extra difficulty in calculating the thickness of the cement annulus or the wave velocity in the cement. Figure 6a shows the calculated flexural-wave attenuation versus the position of the defect. We can see that the measured flexural-wave attenuation depends on the acoustic impedance of the material behind the casing between the two receivers. When the 10 cm length defect exactly located between the two receivers, the measured flexural-wave attenuations drop to 0.5 dB/cm that was obtained in the case with homogeneous water behind the casing. When the defect partly overlaps the spacing between the two receivers, the measured attenuations are proportional to the overlap length. A defect located between the transmitter and the near receiver may slightly change the measured flexural-wave attenuation. The reason is that reflections caused by the interfaces of the defect can change the shape of the envelope. The group velocity of the

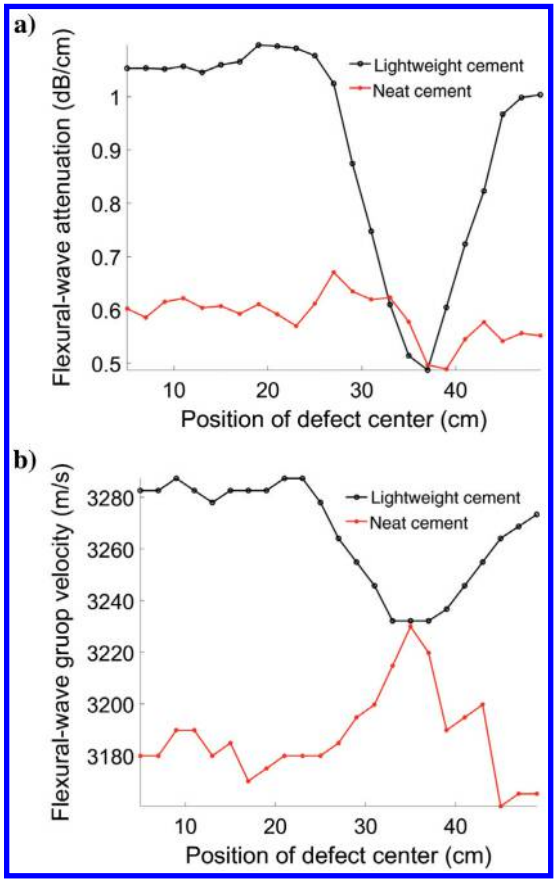

Figure 6. The (a) attenuation and (b) group velocity of the flexural wave versus the position of the defect center.

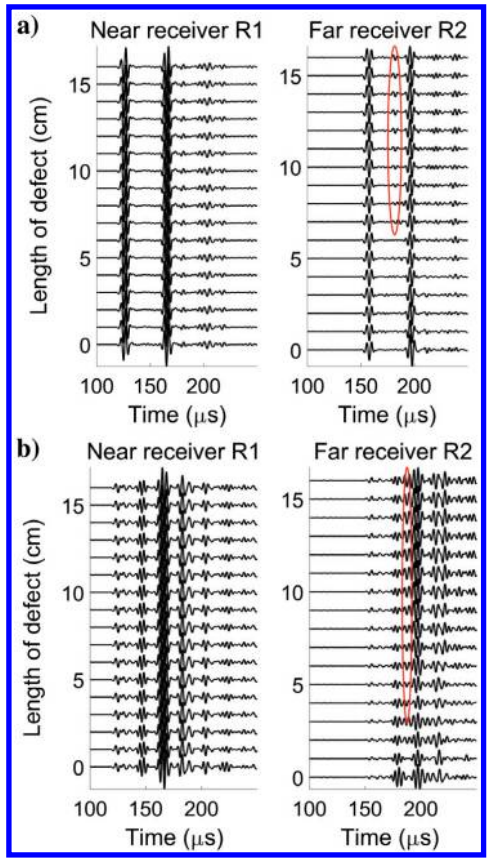

Figure 7. Simulated waveforms for a defect with varying length in cement next to the casing located between R1 and R2. (a) Neat cement and (b) lightweight cement.

flexural wave is shown in Figure 6b. As the receivers pass through the defect, the group velocity of the flexural wave for lightweight cement gradually decreases to 3230 m/s, and then it increases back to 3280 m/s. Likewise, for neat cement, the group velocity first increases to 3230 m/s and then drops back. In addition to the attenuation rate, the group velocity of the flexural wave can be used in evaluation of cement defects.

The effects of the defect length

The recorded flexural waves with various void sizes are investigated. A water-filled void of 2 cm in thickness is located next to the casing. The x-coordinate of the left edge of the void is at 30 cm and remains unchanged, and the length changes from 0 to 16 cm. The simulated waveforms are shown in Figure 7. The scattering from the defect-cement interface is only present in waveforms received by R2, as indicated in the red ellipses, for neat and lightweight cement. For neat cement shown in Figure 7a, the defect scatterings are clear and getting stronger with the increasing defect length. For the lightweight cement shown in Figure 7b, the defect scatterings emerge in between the PP and PS modes of TIE and there are no distinct wave packets. Figure 8a shows the flexural-wave attenuation changes with the defect length. For lightweight cement, the flexural-wave attenuation deceases linearly as the defect length increases. The resolution of the logging tool is determined by the distance between R1 and R2. It is reasonable that once the defect length exceeds that resolution size, the measured attenuation and group velocity stop changing. However, for neat cement, we obtained a misleading attenuation rate when the defect length is less than 10 cm. This may be caused by the coexistence of defect and cement that slightly changes the envelope shape of the primary flexural wave of R2. Figure 8b shows the group velocity of flexural waves versus defect length. For both cases, the group velocity gradually changes to 3230 m/s as the defect length increases. We can see that group velocity is a more reliable parameter for distinguishing neat cement and water.

The effects of defect thickness

Figures 9 and 10 show how the flexural waves are influenced by the thickness of a water-filled void. The void length is 12 cm, and its center is located at $x = 36$ cm. The defect thickness varies from 0 to 1 cm. For cases in which the defect thickness is less than 3 mm, a finer grid size (0.25 mm) and time step (0.024 μs) are used to ensure that there are at least four grid points in the thickness direction. In the right panel of Figure 9a for neat cement, the defect scattering separates from the primary flexural waves and TIE gradually as the defect thickness increases, as indicated by the red lines. In Figure 9b for lightweight cement, by comparing the uppermost waveforms of R1 and R2, one can see that the defect scattering distorts the TIE

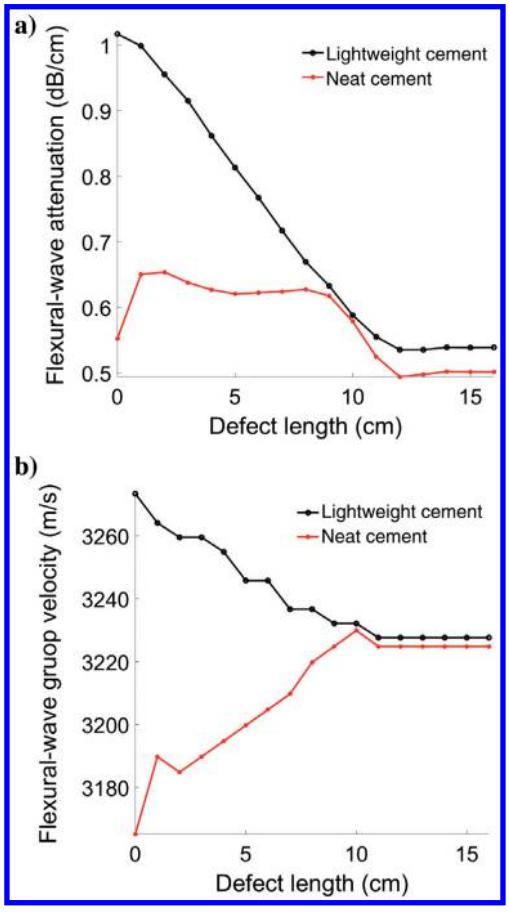

Figure 8. The (a) attenuation and (b) group velocity of the flexural wave versus the defect length.

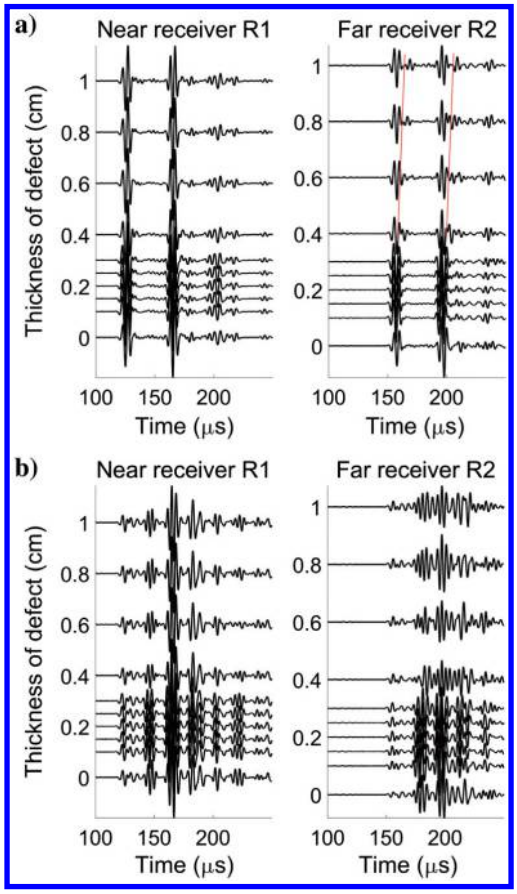

Figure 9. Simulated waveforms for a defect with varying thickness in cement next to the casing located between R1 and R2. (a) Neat cement and (b) lightweight cement.

packets. Figure 10a shows that the measured attenuations oscillate toward the attenuation with water behind the casing as the defect thickness increases, for lightweight and neat cement. A defect with thickness larger than 3 mm can lead to the measured attenuation close to the one with water behind the casing. The curves of the group velocity shown in Figure 10b have similar behaviors as those in Figure 10a as the defect thickness increases.

The effects of an inner defect

We then place a 12×1 cm water-filled void inside the cement layer. The void center is located at $x = 36$ cm. Note that the void does not make contact with the casing. Its distance from the casing is defined by the distance away from the casing, also called the burial depth. In Figure 11a for neat cement, the defect scatterings from the upper and bottom interfaces of the void are indicated by two red parallel lines. For the lightweight cement shown in Figure 11b, the defect scatterings are not discernible due to the superposition of defect scatterings and TIEs. When the void burial depth is 3–4 mm, the defect scatterings partly overlap with the primary flexural wave but have different phases, which greatly distorts the primary flexural-wave envelope and leads to an unreasonable attenuation rate and group velocity for neat and lightweight cement (see the wave packets in the two ellipses in Figure 11 and the curves in Figure 12). When the burial depth is no less than 5 mm, the attenuation and group velocity are close to the values with the homogeneous cement behind the casing. The inner defect cannot be detected by the attenuation rate or group velocity of flexural waves. However, the defect scatterings can indicate the existence of the defect. For neat cement, the burial depth of an inner defect can be calculated by using the time difference between the primary flexural wave and the first defect scattering. The thickness of the defect can be calculated by using the time difference between the first and the second defect scattering. The length of the defect can be estimated by using the amplitude of the defect scatterings.

DISCUSSION

The flexural-wave attenuations for water and neat cement are close to each other and difficult to identify only using flexural-wave attenuation. The imaging behind the casing technology proposed by Schlumberger combines flexural-wave attenuation and acoustic impedance measured by pulse-echo logging to address the difficulty. Because the group velocity can be measured with high precision, this provides an alternative solution. Combining flexural-wave attenuation and the group velocity also allows a discrimination between solids and liquids. Because the acoustic-impedance measurement is more susceptible to the downhole environment, the use of the flexural-wave group velocity can also enhance the reliability in

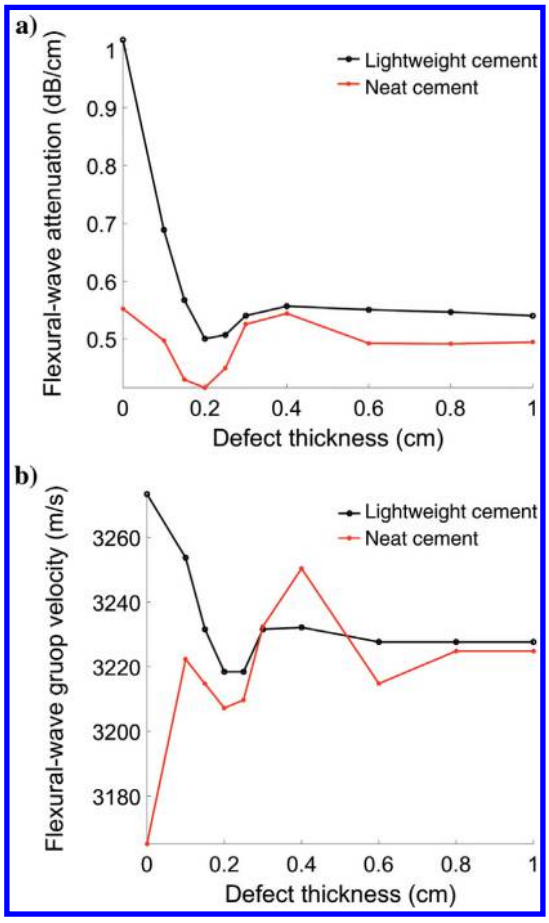

Figure 10. The (a) attenuation and (b) group velocity of the flexural wave versus the defect thickness.

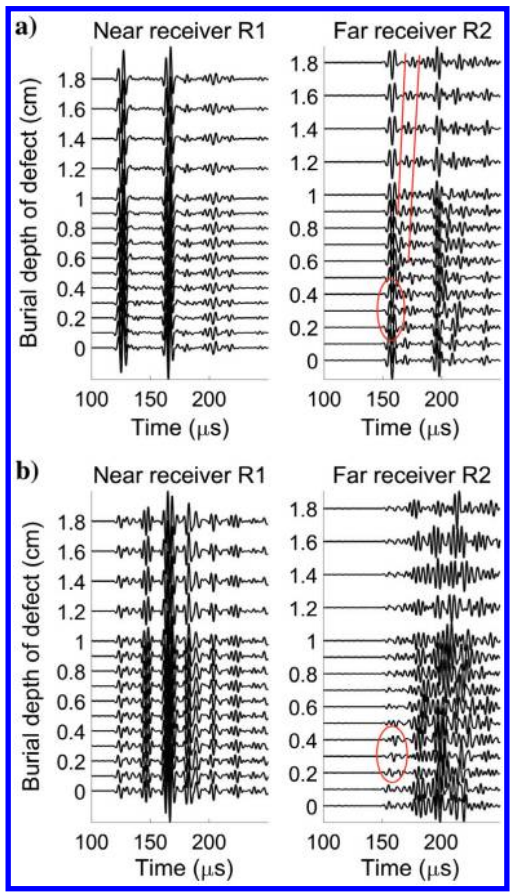

Figure 11. Simulated waveforms for an inner defect with varying distance away from the casing located between R1 and R2. (a) Neat cement and (b) lightweight cement.

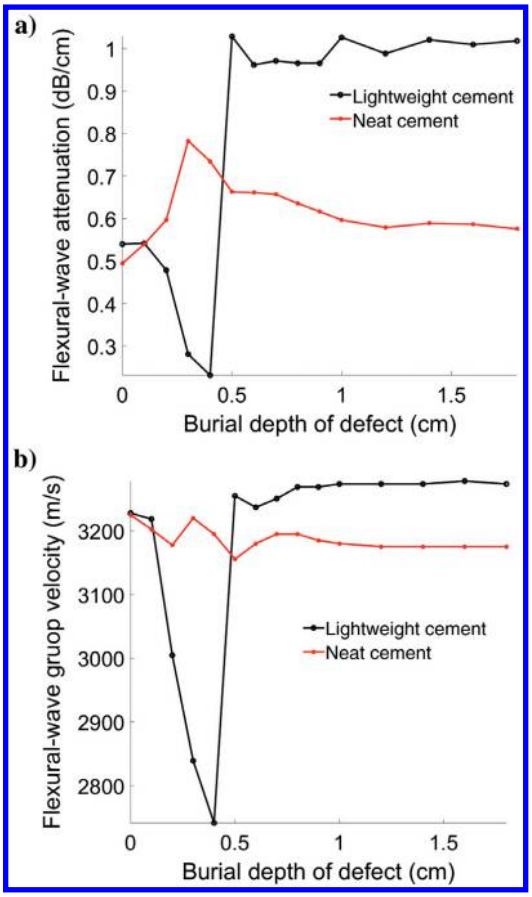

Figure 12. The (a) attenuation and (b) group velocity of the flexural wave versus the burial depth of the defect.

the determination of zonal isolation using imaging behind casing technology.

An inner defect with a burial depth of no less than 5 mm cannot be detected using this approach. However, the defect-induced scattering can be used to indicate the existence of an inner defect and even to characterize defect geometry for neat cement. In actual field scenarios, a fluid channel in the cement-formation interface is more common than a fluid channel contacting with the casing. It is significant to dig into the defect scatterings to image the inner defects.

CONCLUSION

This paper examines the effects of a water-filled void in neat and lightweight cement behind the casing on the attenuation, group velocity, and reflections of flexural waves using the 2D numerical method. The numerical results obtained in this study provide an improved understanding of flexural-wave logging results. Furthermore, from the numerical results, we have two new findings. The first finding is that the flexural-wave group velocity also depends on the material immediately behind the casing. The flexural-wave group velocity is 3180, 3230, and 3280 m/s for neat cement, water, lightweight cement behind the casing, respectively, this allows a discrimination between cement and fluid-filled defect. The use of flexural-wave group velocity can enhance the reliability in the determination of zonal isolation using flexural-wave logging technique. The second finding is that the defect-induced scattering can be used to indicate the existence of an inner defect (a defect that is not contacting with the casing). For neat cement, the arrival time and amplitude of defect-induced scattering can be used to characterize the defect geometry.

ACKNOWLEDGMENTS

The authors wish to express their hearty thanks to the reviewers and editors for their constructive comments and their help in English.

DATA AND MATERIALS AVAILABILITY

Data associated with this research are available and can be obtained by contacting the corresponding author.

REFERENCES

Al-Suwaidi, A. S., F. Al-Marri, E. Sultan, K. Jammeli, Z. Al-Kindi, and A. Elkadi, 2009, Increased certainty in the determination of zonal isolation through the integration of annulus geometry imaging and improved solid-fluid discrimination: The 16th SPE Middle East Oil & Gas Show and Conference, SPE 120061.

Al-Suwaidi, A. S., C. Hun, J. L. Bustillos, D. Guillot, J. Rondeau, P. Vigneaux, H. Helou, J. A. M. Ramirez, and J. L. R. Robles, 2001, Light as a feather, hard as a rock: Oilfield Review, **13**, 2–15.

Froelich, B., 2008, Multimode evaluation of cement behind steel pipe: Journal of the Acoustical Society of America, **123**, 5023–5028.

He, X., H. Chen, and X. M. Wang, 2014, Ultrasonic leaky flexural waves in multilayered media: Cement bond detection for cased wellbores: Geophysics, **79**, no. 2, A7–A11, doi: 10.1190/geo2013-0361.1.

Kuijk, R., S. Zeroug, B. Froelich, M. Allouche, S. Bose, D. Miller, J. Calvez, V. Schoepf, and A. Pagnin, 2005, A novel ultrasonic cased-hole imager for enhanced cement evaluation: International Petroleum Technology Conference, Expanded Abstracts, 10546.

Liu, Q. H., E. Schoen, F. Daube, C. Randall, H. L. Liu, and P. Lee, 1996, A three-dimensional finite difference simulation of sonic logging: Journal of the Acoustical Society of America, **100**, 72–79, doi: 10.1121/1.415869.

Song, R. L., J. X. Liu, C. H. Hou, and K. X. Wang, 2012, Numerical simulation of sector bond log and improved cement bond image: Geophysics, **77**, no. 4, D95–D104, doi: 10.1190/geo2011-0273.1.

Tao, B., D. H. Chen, X. He, and X. M. Wang, 2016, Rough interfaces and ultrasonic imaging logging behind casing: Applied Geophysics, **13**, 683–688, doi: 10.1007/s11770-016-0576-7.

Wang, H, G. Tao, and X. F. Shang, 2016, Understanding acoustic methods for cement bond logging: Journal of the Acoustical Society of America, **139**, 2407–2416, doi: 10.1121/1.4947511.

Wang, T., and X. M. Tang, 2003, Finite-difference modeling of elastic wave propagation: A nonsplitting perfectly matched layer approach: Geophysics, **68**, 1749–1755, doi: 10.1190/1.1620648.

Xu, F. L., and H. S. Hu, 2017, Inversion of the shear velocity of the cement in cased borehole through ultrasonic flexural waves: Geophysics, **82**, no. 2, D57–D68, doi: 10.1190/geo2016-0314.1.

Zeroug, S., 2004, Forward modeling for ultrasonic leaky lamb-wave based imaging through a highly contrasting steel cylindrical layer: IEEE Ultrasonics Symposium, Expanded Abstracts, 672–675, doi: 10.1109/ULTSYM.2004.1417812.

Zeroug, S., and B. Froelich, 2003, Ultrasonic leaky-lamb wave imaging through a highly contrasting layer: IEEE Ultrasonics Symposium, Expanded Abstracts, 794–798, doi: 10.1109/ULTSYM.2003.1293520.